Hindawi
Shock and Vibration
Volume 2019, Article ID 4525798, 10 pages
https://doi.org/10.1155/2019/4525798

Research Article

Effect of Structure Parameters on Polycal Wire Rope Isolator Stiffness-Damping Characteristics

Shaowu Tu, Xiaofeng Lu, and Xiaolei Zhu

School of Mechanical and Power Engineering, Nanjing Tech University, Nanjing 211800, China

Correspondence should be addressed to Xiaofeng Lu; xflu@njtech.edu.cn and Xiaolei Zhu; zhuxiaolei@njtech.edu.cn

Received 19 December 2018; Revised 3 March 2019; Accepted 5 May 2019; Published 2 June 2019

Academic Editor: Gilbert R. Gillich

Wire rope isolators are mainly used to isolate vibration and protect precise equipment. However, the issue of regulation of vibration isolators taking into account the nonlinearity of their characteristics was poorly understood in the modern literature. In this paper, the influence of structural parameters (diameter ratio and lay pitch of the single strand, and lay pitch and bending radius of the wire rope) on stiffness-damping characteristics of the Polycal WRI was investigated by the simplified finite element analysis method. The stiffness and damping prediction models including structural parameters and material properties were established. The results showed that the stiffness-damping characteristics were the best; when the diameter ratio of wire strand was 1.1, the inside layer wire pitch length was 6 times the diameter of the wire strand, the outside layer wire pitch length was 11 times the diameter of the wire strand, the pitch length of the wire rope was 7.5 times its diameter, and the bending radius was equal to 46.5 mm. The errors of the prediction for prestiffness and softened stiffness were within 5%, and the errors of prediction for the energy dissipation coefficient were within 10%.

1. Introduction

Vibration is common in our lives. Especially in many industries, vibration is caused by the equipments operation, fluid flushing in pipes, and aero engine. This is harmful for operation safety [1–3]. Many vibration reduction and vibration suppression methods have been studied. Vibration isolators are widely applicable to production and living. Particularly, it is widely used in equipments with high load and vibration reduction requirements. In recent years, new type of vibration isolators and design of vibration isolation systems are hot topic for scholars. Wire rope isolator (WRI) has excellent rigidity damping characteristics, especially with high bearing capacity. It is widely used in mechanical manufacturing and construction. Therefore, it is necessary and significant to study the characteristics of the WRI with different structural parameters.

The characteristics of the WRI are studied through the experimental and theoretical methods [4–11]. Chen et al. [12] investigated the contact statues of a steel wire rope from the perspective of theoretical analysis. The result shows that the effect of the lay angle on the stiffness of the wire rope is different under different loads. Tinker and Cutchins [13] obtained the data of stiffness and damping characteristics of the WRI through dynamic experiment. It is also found that the damping of the WRI is related to coulomb-type friction. Demetriades et al. [14] studied the response characteristics under different loads for different structures of the WRI. The result indicated that the WRI exhibits the same characteristics under shear and roll loads. Wang et al. [15] experimentally investigated the effects of load frequency, amplitude and structural parameters on the dynamic characteristics of O-type WRIs. He found that the loading amplitude and geometric parameters of the isolator directly affects the dynamic characteristics of the isolator, while the loading frequency has no effect on it. Gerges [9] investigated the tension-compression mode of the wire rope spring. He presented a semianalytical model for a wire rope vibration isolator through experiment. Rashidi and Ziaei-Rad [7] investigated the quasi-static and dynamic characteristics of the WRI. It is suggested that there is not obviously relationship between hysteresis loops and loading velocity

under quasi-static load. The dynamic results indicated that by increasing the frequency of excitation, the area of the hysteresis loop starts decreasing. Finally, a hysteresis analytical prediction model with high coincidence degree was established.

The finite element analysis method can reduce the cost of the experiment, and thus has been widely used in studying the characteristics of the WRI and wire ropes. Jiang et al. [16] found effective simplified finite element analysis method of analyzing the contact statues of wire ropes. It was found that the local contact deformation affects the accuracy of the results. Wang et al. [17] investigated the mechanical behavior of the YS9-8 × 19 braided wire rope under tensile load. By comparing the results of finite element analysis and experiment, the error between them was small, and the accuracy of the model was verified. By the finite element method, Xiang et al. [18] obtained the elastic-plastic contact stresses under axial and torsion loads of wire ropes, and investigated the elastic-plastic behavior of it. The finite element analysis results have a good agreement with the experimental test results, and a new prediction model was proposed. Yu et al. [19] applied the beam finite element method to analyzing axial tensile properties of the 91-wire strand. By comparing with the experiment results, the beam FEM could be used to predict the tensile properties of the steel wire rope. Song et al. [20] analyzed distributions of stress and deformation in the braided wire rope subjected to torsional loading. He found that the wires in the strands have the tendency to be screwed tightly and are in a stretched state when the lay direction of the strand coincides with its torsion direction. Cao and Wu [21] established the finite element model of wire ropes with different structural parameters and analyzed the stress distribution and deformation under cantilever beam state. The accuracy of the results of finite element analysis was slightly lower than the theoretical calculation results. Du et al. [22] presented a simulation of the 6 × 36 + WS RHRL wire rope. It is found that the stress of the wire rope was uneven, and the maximum stress occurs at the side of the wire. Yong et al. [23] conducted a finite element analysis of the IWRC6 ∗ 36WS wire rope, and the elastic behavior of the wire rope under tensile loads was simulated. It is reported that nonlinear relationship between the axial tension and the axial elongation of the wire rope. Cen et al. [24] found effective simplified finite element analysis method by combining finite element method with experimental test. This method can be used to analyze the characteristics of the Polycal WRI. The above studies have studied the characteristics of wire ropes and vibration isolators by experiments and finite element methods and obtained some results. Considering the complexity of the wire rope isolator structure, there is less research on the relationship between the structural parameters of the WRI and the stiffness and damping characteristics of the WRI. Therefore, it is necessary to study the relationship between them, and provide guidance for practical engineering applications.

In this paper, the stiffness and damping characteristics of WRIs with different structural parameters were investigated. These structural parameters were number of wire ropes, material of wire, rope diameter (D), rope lay pitch (P), single wire rope diameter (d), single wire strand lay pitch (p_{in}, p_{out}), and wire rope diameter ratio (n_r). A stiffness-damping prediction model consists of structural parameters of the Polycal WRI were established, which aims to provide powerful help for the structural design and wire rope selection of the Polycal WRI.

2. Method

2.1. Energy Dissipation Coefficient. The energy dissipation coefficient is a key parameter evaluating the effective vibration isolation property of a WRI. It is an important reference for evaluating the damping characteristics of the WRI. Because of sliding friction between the wire strands and the internal friction of wires, the isolators exhibit nonlinear hysteretic behavior. Typical load-displacement curve of the WRI is shown in Figure 1. The damping characteristics of the WRI are related with the area which is enclosed by the loading and unloading curve of the WRI under compression. The energy dissipation coefficient C was calculated as follows:

$$C = \frac{A_{loop}}{\pi\left(\left(F_{max} - F_{min}\right)/2\right)\left(\left(X_{max} - X_{min}\right)/2\right)}, \quad (1)$$

where A_{loop} was the area of the hysteresis loop (N·mm), F_{max} and F_{min} were the maximum and minimum loads (N), respectively, of the WRI in the compression loading-unloading process. X_{max} and X_{min} were the maximum and minimum displacement (mm) in the loading-unloading process.

In most of the wire rope isolators, during the load-bearing process, the upper and lower pallets are mainly supported by the curved steel wire rope, and the bending stiffness and deformation process of the steel wire rope play a decisive role. Therefore, this paper mainly uses the stiffness and energy dissipation coefficient as indicators to measure the effectiveness of the wire rope isolators.

2.2. Calculation Method and Finite Element Model

2.2.1. Calculation Method. As shown in Figure 2(a), the WRI was composed of two pallets and twelve 6 × 19 IWS wire ropes. In this paper, the simplified finite element method is used to obtain the WRI load-displacement hysteresis loop, and the WRI stiffness damping of different structural parameters is discussed. We have referenced the simplified finite element method which was established by Cen et al. [24]. This method mainly simplified the single strand into a single wire. The 6 × 19 IWS wire rope was simplified into the 1 × 7 wire rope, as presented in Figure 2(b). Based on the simplified method, this paper studies the stiffness and damping characteristics of the isolators with different structural parameters and establishes the prediction model of the stiffness damping of the wire rope isolator with structural parameters as variables.

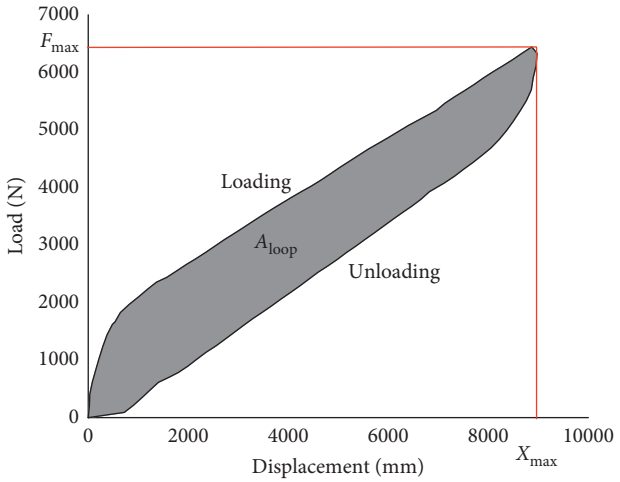

Figure 1: The typical load-displacement curve of the WRI.

2.2.2. Definitions of Finite Element Model. This paper is mainly based on the GGQ-99 Polycal WRI. By changing structural parameters, the diameter ratio and lay pitch of the single strand and lay pitch and bending radius of the wire rope, different finite element models were set.

In this presented model, the data source of the simulation of the WRIs refers to papers of Cen et al. [24], Jiang et al. [25], and Erdonmez and Imrak [26]. The material properties of the center and side wires are defined by the bilinear elastic-plastic kinematic hardening model in the ABAQUS material library, as shown in Table 1. By compression of corresponding strands, the max equivalent compression stress of the strand and equivalent compression elastic modulus are equal to σ_{Ay} and E_p, respectively. E_e is equal to the equivalent tension elastic modulus which is measured by the tension of the strands. The density is $\rho = 7850\,\text{kg}\cdot\text{m}^{-3}$, and the Poisson's ratio is $\mu = 0.3$ [24].

In the general contact type, the All with self is selected to define the contact type between the center strand and lay strand. The tangential behaviour with the penalty friction coefficient is 0.115 and normal behaviour with hard contact [25, 26]. The mesh type is a 3D solid linear reduction integration unit (C3D8R). The down-pallet is fully constrained, and the up-pallet is constrained except for the displacement load applied in the vertical direction.

3. The Analysis of WRI Stiffness-Damping with Different Structural Wire Ropes

The stiffness of the WRI determines the load-bearing capacity of the vibration isolation system, regardless of whether the WRI is subjected to a static load or a strong impact load. The softening load of the WRI and the subsequent softening stiffness both affect the efficiency of vibration isolation and stability of the entire isolator system. The damping characteristic reflects the ability to absorb shock vibration energy of the isolator in the vibration isolation system. There are many factors that affect the static stiffness and damping characteristics of the WRI, including the selection of the wire rope, number of wire ropes, material of steel wire, wire rope diameter (D), rope lay pitch (P), single wire rope diameter (d), single wire strand lay pitch (p_{in}, p_{out}), wire rope diameter ratio (n_r), and arc wire rope bending radius (R).

3.1. Wire Rope Diameter Ratio. As shown in Figure 3, the diameter ratio (n_r) of the 1 + 6 + 12 center strand or the lay strand is defined as follows:

$$n_r = \frac{r_c}{r_s}, \tag{2}$$

where r_c and r_s are the diameters of the center wire and lay wire in the single strand, respectively.

Figure 3 shows the 1 + 6 + 12 single-strand wire rope. It was stipulated that the 1 + 6 + 12 single-strand wire rope has the same other structural parameters; the first layer wire pitch length was 6 times the diameter of the single wire rope, and the second layer wire pitch length was 11 times the diameter of the single wire rope. The diameter of the wire rope was 8 mm in the study of the GGQ-99 Polycal WRI. The diameter of the center strand was 2.839 mm, and the diameter of the lay strand was 2.581 mm. Obviously, the former was 1.1 times more than the latter. The lay pitch length was 60 mm (7.5 times diameter of the wire rope), and the bending radius was 46.5 mm of the arc wire rope. The diameters of the center wire and lay wire in different strands with different diameter ratios of the GGQ-99 are listed in Table 2.

According to the simplified FEM model, the tensile and compression of the single strand with different diameter ratios were calculated. The elastic tensile and compression modulus and compression ultimate load of the single strand were obtained. These mechanical parameters were used to calculate the stiffness-damping characteristics of the WRI. It is presented in Table 3. It could be seen that the elastic tensile modulus significantly reduced with increased diameter ratio. But the elastic compression modulus increased with increased diameter ratio. The compression ultimate load is kept steady basically with increased diameter ratio. The reason is that the compression ultimate load indicated the friction properties between the center wire and lay wire. The friction between the center wire and lay wire was retained about the same during calculating the model with different diameter ratios. So, the compression ultimate loads showed little changes.

According to the simplified FEM model, the compression loading-unloading processes of the GGQ-99 WRI with different diameter ratios were simulated. Different load-displacement hysteresis loop curves of the WRI are shown in Figure 4. The ratio between the prestiffness K_1 and softened stage stiffness K_2 indicated the impact resistance for the WRI. The smaller this value, the better the impact resistance. The energy dissipation coefficient was used to evaluate the damping characteristic. The higher this value, the better the damping characteristic. The results are shown in Figure 5.

As shown in Figure 4, the compression load of the WRI increased with increasing of the diameter ratio of the wire

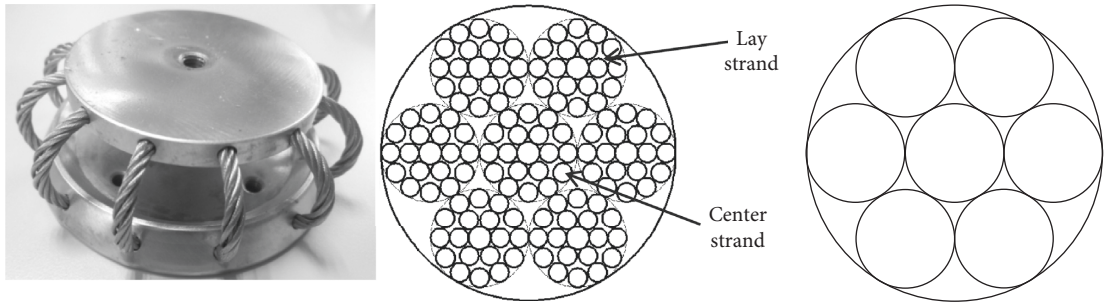

Figure 2: WRI structure: (a) GGQ-99 WRI; (b) simplified model of 6×19 IWS wire ropes.

Table 1: Material parameters of the kinematic hardening model for the arc wire rope [24].

Arc strand	E_e (GPa)	E_p (GPa)	σ_{Ay} (MPa)
Center wire	64.25	10.66	16.80
Side wire	80.37	10.68	18.34

Reproduced from Cen et al. [24] (under the Creative Commons Attribution License/public domain).

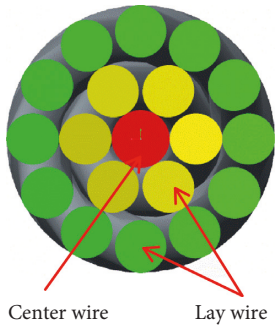

Figure 3: The 1 + 6 + 12 single-strand wire rope.

Table 2: Diameter of wire for single strands with different diameter ratios (mm).

Diameter of wire	n_r				
	1.1	1.2	1.3	1.4	1.5
Center strand					
Center wire	0.614	0.655	0.696	0.736	0.774
Lay wire	0.556	0.546	0.536	0.526	0.516
Lay strand					
Center wire	0.557	0.595	0.633	0.669	0.704
Lay wire	0.506	0.496	0.487	0.478	0.469

Table 3: The mechanical parameters of single strands with different diameter ratios.

FEM results of single strand	n_r				
	1.1	1.2	1.3	1.4	1.5
Center strand					
E_t (GPa)	70.10	63.25	60.58	59.52	57.29
E_c (GPa)	11.52	12.38	13.48	14.80	15.94
σ_{max} (MPa)	17.50	16.21	16.16	16.54	16.33
Lay strand					
E_t (GPa)	77.61	69.16	67.05	65.73	61.94
E_c (GPa)	11.80	12.45	13.52	14.87	16.00
σ_{max} (MPa)	17.78	16.41	16.15	16.93	16.77

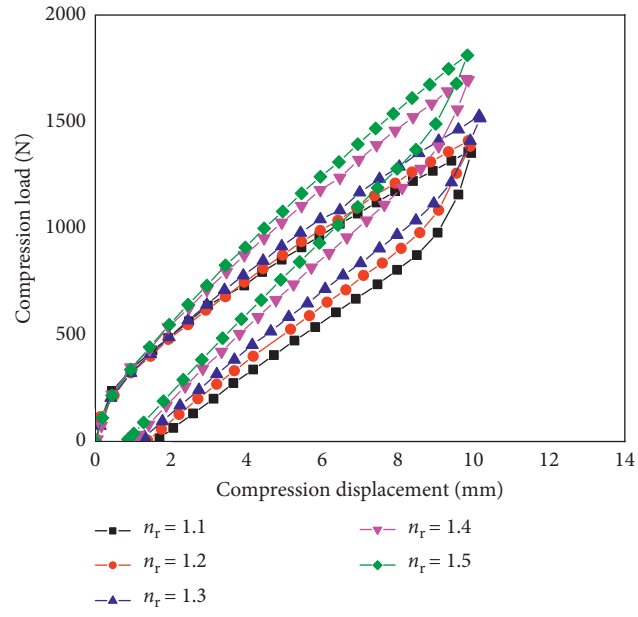

Figure 4: Hysteresis curves comparison of the GGQ-99 WRI with different diameter ratios.

strand. This result is related to the elastic compression modulus of the single strand. As shown in Figure 5, the ratio of K_1 to K_2 was increased with increasing of the diameter ratio of the wire strand. The ratio of K_1 to K_2 reached the minimum when the diameter ratio was equaled to 1.1. It means that the GGQ-99 WRI was easier to maintain the stability of the vibration isolation system through large deformation. The energy dissipation coefficient for the WRI decreased with increasing of the diameter ratio of the wire strand. When the ratio of the strand was equaled to 1.1, the energy dissipation coefficient reached maximum. These results indicate that the Polycal WRI has better damping characteristics, which could effectively consume the impact load and eliminate the vibration from the isolation system.

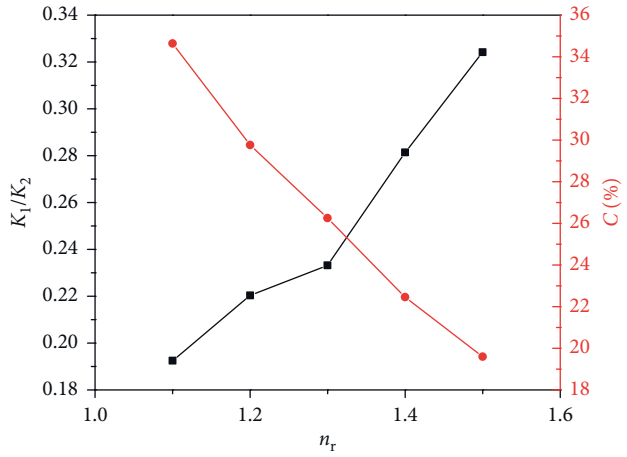

Figure 5: Relationship between stiffness ratio and energy absorption coefficient with different diameter ratios.

3.2. Lay Pitch of Single Strand. Based on the diameter ratio of the wire strand to 1.1, the main purpose of this section is to study the effect of the outer layer side wire pitch length (p_{out}) on the stiffness-damping of the Polycal WRI. During the process of creating the simulation model, the first layer side wire of the strand steel wire rope (p_{in}) was unchanged and equal to 6 times the diameter of the wire strand. The p_{out} was 7 times, 8 times, 9 times, 10 times, and 11 times the diameter of the wire strand. The relation between the pitch length and diameter of the wire strand (d) is expressed in equation (3). The geometric dimensions of the single wire strands with different pitch lengths are shown in Table 4.

$$t = \frac{p_{out}}{d}. \tag{3}$$

As shown in Table 5, the equipment tensile modulus, compression modulus, and softened stress of the wire strands with different p_{out} were obtained by axial tension and compression. The modulus of the tension was continuously increased with increasing of the outer layer side wire pitch. The modulus of the compression had a small variation with increasing of the outer layer side wire pitch basically, and the maximum load of the corresponding compression process decreased.

The equipment tensile and compression performance of wire strands with different p_{out} were used to define the bilinear elastic-plastic kinematic hardening material properties of the center and lay strand assembled in the GGQ-99 WRI. As shown in Figure 6, the load-displacement hysteresis loops of different lay pitches had a small variation. Besides, the modulus of the compression was not changing with increasing of the outer layer side wire pitch. Combined stiffness-damping characteristics of the GGQ-99 WRI with the different wire strand pout are shown in Figure 7. When the p_{out} was 11 times the diameter of the wire strand, the ratio of K_1 to K_2 reached the minimum. At the same time, the Polycal WRI had large prestiffness and the most obvious softening characteristics, not only could withstand large loads but also could easily maintain the stability of the vibration isolation system through large deformation under the action of large loads. The energy dissipation coefficient of the WRI remained basically unchanged, when the ratio of the outside lay pitch and the diameter of the strand increased.

Table 4: The geometric dimensions of the single wire strands with different pitch length (mm).

Pitch length	p_{in}	p_{out}				
		$t=7$	$t=8$	$t=9$	$t=10$	$t=11$
Center strand	17.034	19.873	22.712	25.551	28.39	31.229
Lay strand	15.486	18.067	20.648	23.229	25.81	28.391

Table 5: The FEM results of single strands with different lay pitches.

FEM results of wire strands	p_{out}/d				
	$t=7$	$t=8$	$t=9$	$t=10$	$t=11$
Center strand					
E_t (GPa)	46.18	48.04	55.59	60.83	70.10
E_c (GPa)	11.82	11.80	11.76	11.41	11.52
σ_{max} (MPa)	25.01	23.08	21.71	19.74	17.50
Lay strand					
E_t (GPa)	52.90	55.48	61.13	66.61	77.61
E_c (GPa)	11.73	11.56	11.85	11.52	11.80
σ_{max} (GPa)	24.49	23.23	21.75	19.80	17.78

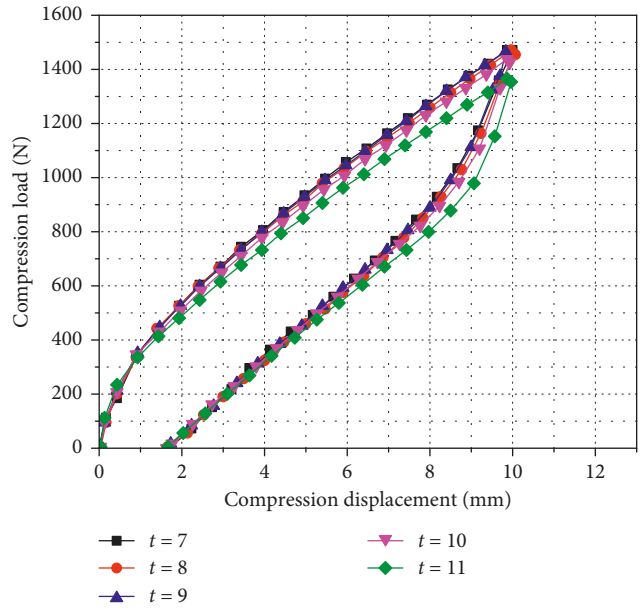

Figure 6: Hysteresis curves comparison of the GGQ-99 WRI with different lay pitches.

3.3. Lay Pitch of Wire Rope. In the process of compression loading-unloading of the Polycal WRI, not only the slippage of the wires exists in the strand but also the overall slippage of the strands in the rope. Therefore, the influence rule of the pitch length on the wire rope is discussed in this section. The diameter ratio, the inside layer wire pitch length and outside layer wire pitch, was equaled to 1.1. It was 6 times the

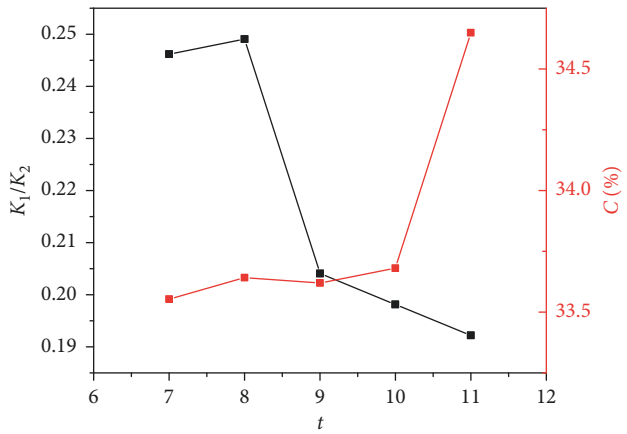

Figure 7: The stiffness-damping characteristics of the GGQ-99 WRI under the lay pitch.

diameter of the wire strand and 11 times the diameter of the wire strand, respectively. The relation between the pitch length and diameter of the wire rope (D) is expressed in equation (4). Table 5 lists the geometric dimensions of the single wire strands with different pitch lengths. The load-displacement hysteresis loops of the GGQ-99 WRI with different pitch lengths are shown in Figure 8.

$$T = \frac{p_{\text{out}}}{D}. \tag{4}$$

As shown in Figure 8, the compression load of the WRI increased with increasing of the pitch length of the wire rope. The increase of the pitch length contributed to the increase of the angle between the center strand and lay strand. The bearing axial load of the lay strand increased with angle between center strand and lay strand decreasing. So, the compression load of the WRI was increased with the increasing of the pitch length of the wire rope.

The stiffness-damping characteristics of the GGQ-99 WRI with different pitch lengths of wire ropes are shown in Figure 9. As shown in Figure 9, both the ratio of K_1 to K_2 and the energy dissipation coefficient of the WRI fluctuated with the increase of the pitch length of the arc rope. When the rope pitch was equaled to 7.5 times the diameter of rope, the ratio of K_1 to K_2 was the smallest and less than 0.2 and the energy dissipation coefficient was the biggest.

3.4. Bending Radius of Wire Rope. The characteristics of the Polycal WRI depend on the structure of the wire rope, including the diameter of the single strand, the pitch length of the single strand, and the bending radius of the wire rope. In this section, the influence of the bending radius (R) of the arc rope on the stiffness-damping characteristics of the Polycal WRI is studied. The diameter ratio of the wire strand was 1.1. The inside layer wire pitch length was 6 times the diameter of the wire strand. The outside layer wire pitch length was 11 times the diameter of the wire strand, and the pitch length of the wire rope was 7.5 times its diameter. The bending radius was equal to 46.5 mm, and the bending radius of the wire rope was 50 mm, 55 mm, 60 mm, and

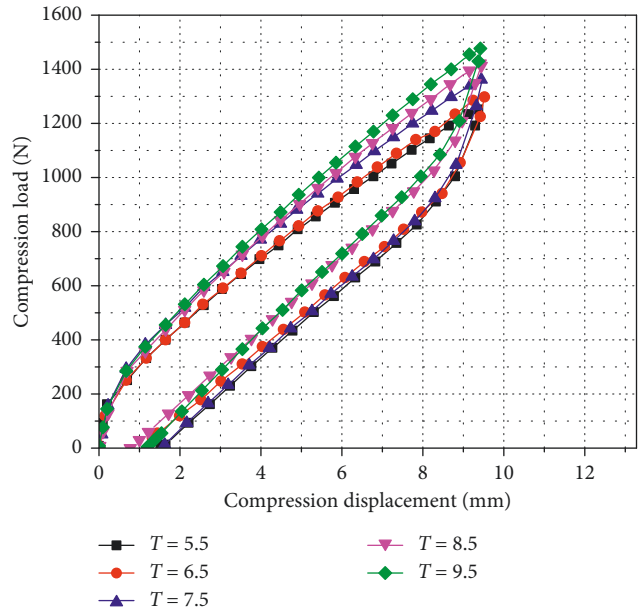

Figure 8: Hysteresis curves comparison of the GGQ-99 WRI with different arc rope lay pitches.

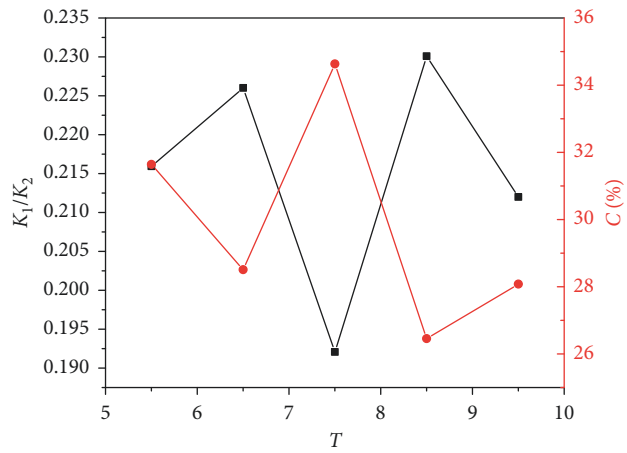

Figure 9: The stiffness-damping characteristics of the GGQ-99 WRI with different pitch lengths of wire ropes.

65 mm, respectively. The FEM models of the GGQ-99 WRI with different bending radii are shown in Figure 10. The load-displacement hysteresis loops of the GGQ-99 WRI with different bending radii of arc ropes are shown in Figure 11.

As shown in Figure 11, the compression load of the WRI increased with increasing bending radius of arc ropes. Because the compression load of the WRI was inversely proportional to the curvature of the wire rope, the curvature of the wire rope decreased with increasing bending radius of arc ropes. The compression load of the WRI increased with increasing bending radius of arc ropes.

The stiffness-damping characteristics of the GGQ-99 WRI with different bending radii of the wire rope are shown in Figure 12. The ratio of K_1 to K_2 increased with increasing bending radius. However, the energy dissipation coefficient of the WRI decreased with increasing bending.

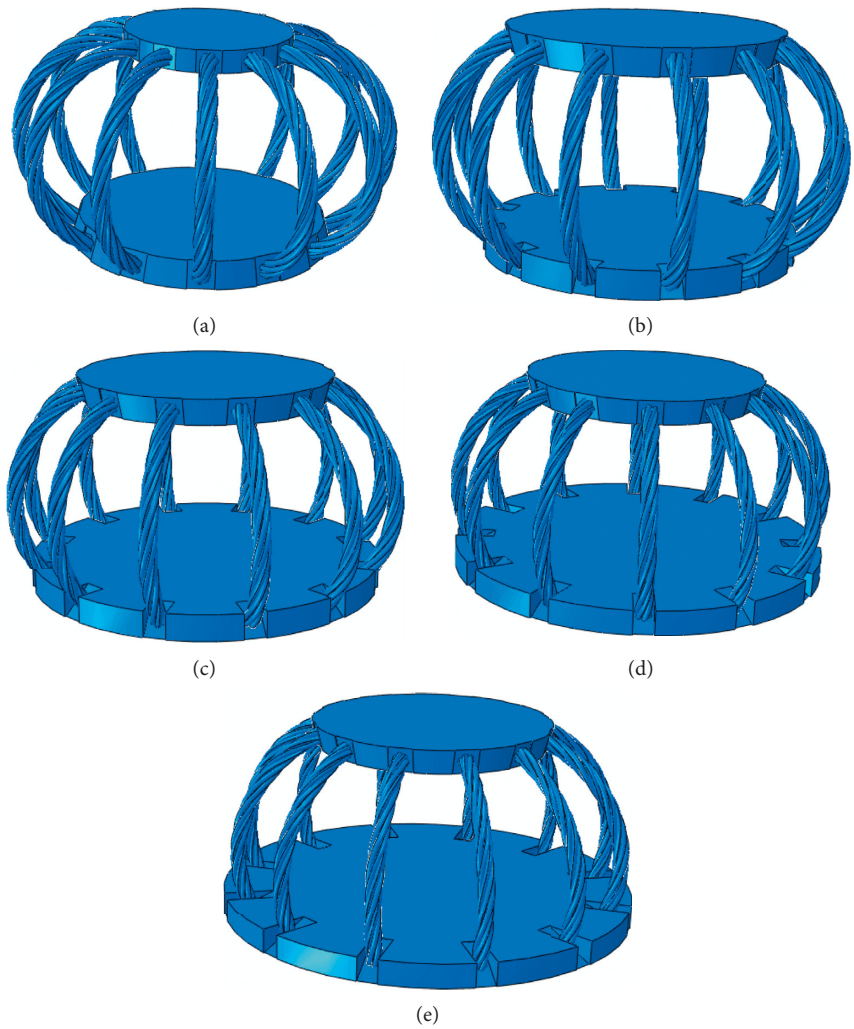

Figure 10: GGQ-99 WRIs with different bending radii. (a) 46.5 mm. (b) 50 mm. (c) 55 mm. (d) 60 mm. (e) 65 mm.

When the bending radius was equal to 46.5 mm, the ratio of K_1 to K_2 was the smallest and the energy dissipation coefficient was the biggest.

In conclusion, the stiffness-damping characteristics were the best; when the diameter ratio of the wire strand was 1.1, the inside layer wire pitch length was 6 times the diameter of the wire strand, the outside layer wire pitch length was 11 times the diameter of the wire strand, and the pitch length of the wire rope was 7.5 times its diameter. The bending radius was equal to 46.5 mm.

4. Stiffness-Damping Prediction Models of WRI

4.1. Prediction Model. In the previous section, the influence rules of the diameter ratio of the wire strand (n_r), the pitch length of the wire strand (p_{in}, p_{out}), the pitch length of the wire rope (P), and the bending radius (R) for the stiffness-damping performance of the Polycal WRI were discussed. The prediction model of the stiffness-damping characteristic of the WRI was established by using the dimensionless diameter ratio of the wire strand (n_r), the pitch length of the wire strand (p_{in}, p_{out}), the pitch length of the wire rope (P), and the bending radius (R). The theoretical basis of equations (5) and (6) is the π theorem in dimensional analysis. According to the principle of dimensional analysis, all structural parameters are transformed into a dimensionless form, and the number of variables is reduced to obtain the corresponding calculation formula as follows:

$$K = kE_1H(n_r)^{x_1}\left(\frac{p_{in}}{p_{out}}\right)^{x_2}\left(\frac{P}{D}\right)^{x_3}\left(\frac{R}{D}\right)^{x_4}, \quad (5)$$

$$C = c(n_r)^{X_1}\left(\frac{p_{in}}{p_{out}}\right)^{X_2}\left(\frac{P}{D}\right)^{X_3}\left(\frac{R}{D}\right)^{X_4}, \quad (6)$$

where E_1 is the elastic modulus of the steel wire material ($E_1 = 193000$ MPa), H is the height of the GGQ-99 WRI ($H = 99$ mm), and D is the diameter of the arc rope ($D = 8$ mm). The x, k, and c are the undetermined coefficients in the stiffness and damping models, respectively.

As shown in Table 6, all values of the prestiffness K_1, softened stiffness K_2, and energy dissipation coefficient C of the GGQ-99 Polycal WRI with different structural parameters were obtained. The coefficient values are listed in

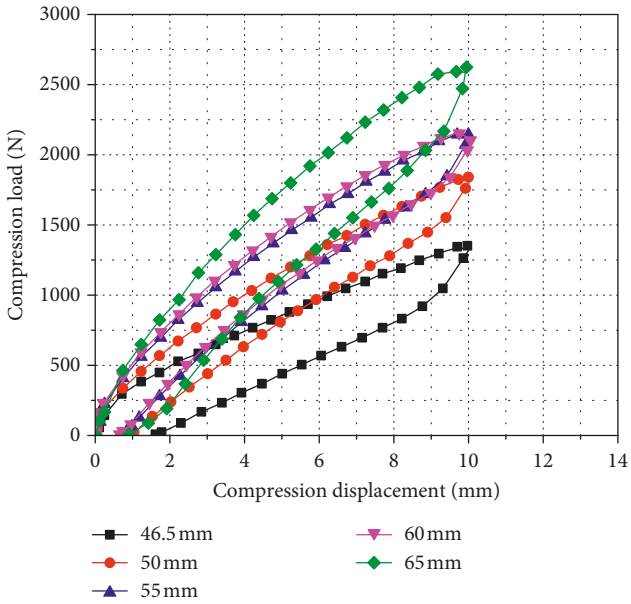

Figure 11: Hysteresis curves comparison of the GGQ-99 WRI with different bending radii.

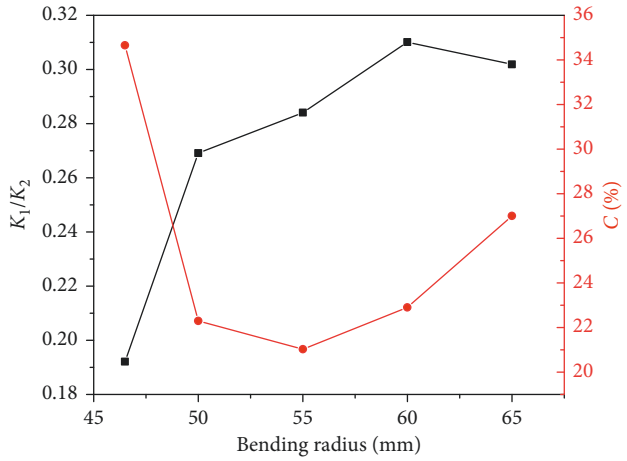

Figure 12: The stiffness-damping characteristics of the GGQ-99 WRI with different bending radii of the wire rope.

Table 7. By using the MATLAB software, equations (5) and (6) were formulated fitting with the corresponding structural parameters, respectively.

4.2. Error Analysis of Prediction Models. As shown in Table 8, the errors of the prestiffness and softened stiffness fitting formulas of the WRI were all within 10%, and more than half of the errors were within 5%. The error of the energy dissipation coefficient of the WRI with the formula was basically within 20%, and more than half of the errors were within 10%. It could be considered that the formula fitted in this study is accurate and reliable by analysing the error results of the overall data. In the design of the Polycal WRI, the stiffness-damping characteristics could be quickly obtained.

Table 6: The stiffness-damping of the GGQ-99 WRI with different structural parameters.

Number	Structural parameters				Stiffness-damping		
	n_r	p_{in}/p_{out}	P/D	R/D	K_1 (N/mm)	K_2 (N/mm)	C (%)
1#	1.1	0.545	7.5	5.8125	564.326	108.341	34.65
2#	1.2	0.545	7.5	5.8125	525.582	115.573	29.76
3#	1.3	0.545	7.5	5.8125	526.628	122.756	26.24
4#	1.4	0.545	7.5	5.8125	541.734	151.971	22.45
5#	1.5	0.545	7.5	5.8125	505.712	163.632	19.63
6#	1.1	0.857	7.5	5.8125	449.583	110.592	33.55
7#	1.1	0.75	7.5	5.8125	439.908	109.667	33.64
8#	1.1	0.667	7.5	5.8125	539.792	110.376	33.62
9#	1.1	0.6	7.5	5.8125	554.747	109.971	33.68
10#	1.1	0.545	5.5	5.8125	484.87	104.764	31.63
11#	1.1	0.545	6.5	5.8125	490.37	110.694	28.49
12#	1.1	0.545	8.5	5.8125	509.811	117.433	26.45
13#	1.1	0.545	9.5	5.8125	590.583	125.242	28.07
14#	1.1	0.545	7.5	6.25	571.113	153.811	22.30
15#	1.1	0.545	7.5	6.875	632.302	179.774	21.03
16#	1.1	0.545	7.5	7.5	569.738	176.736	22.90
17#	1.1	0.545	7.5	8.125	749.393	226.096	26.99

Table 7: The coefficient values after the formula was fitted.

Stiffness-damping	Coefficient				
	x_1/X_1	x_2/X_2	x_3/X_3	x_4/X_4	k/c
K_1	−0.1147	−0.3926	0.3223	0.7524	$3.11e-6$
K_2	1.0194	−0.1066	0.3003	2.0788	$7.15e-8$
C	−1.0778	0.4142	−0.2272	−0.7828	2.614

In order to evaluate the accuracy of the prediction model, the experimental results of Cen et al. [24] were referenced. In his paper, the static compression experiment of GGQ25-62 was studied.

The wire rope structural parameters of the GGQ25-62 Polycal WRI are given in Table 9. Besides, the values of H, D, and R are 62 mm, 4.68 mm, and 27.15 mm, respectively.

As shown in Table 10, the structural parameters of GGQ25-62 were processed in the form of the fitting formula.

Through the out-of-plane compression loading-unloading experiment of the WRI, its stiffness-damping characteristics were obtained. Figure 13 shows the load-displacement curve of the GGQ25-62WRI, and the values of K_1, K_2, and C could be calculated from this figure, and Table 10 also shows the specific values.

Figure 13 is reproduced from the work of Cen et al. [24] (under the Creative Commons Attribution License/public domain).

The fitted value was compared with experimental data. As shown in Table 11, the errors of the prestiffness and softened stiffness fitting formulas of the WRI the values were all within 20%. The reason for this phenomenon is that the finite element is an analysis under ideal conditions. During the test, the vibration isolator is in a complex state, and there will be some nonlinearity characteristics. Therefore, it can be seen that the predicted value given by the prediction model is in good agreement with the experimental value.

Table 8: The fitting error of the stiffness-damping of the WRI with different structural parameters.

Number	Fitted value			Error (%)		
	K_1 (N/mm)	K_2 (N/mm)	C (%)	K_1	K_2	C
1#	536.828	114.165	29.27	−4.87	5.38	−15.54
2#	531.497	124.754	26.65	1.12	7.94	−10.47
3#	526.639	135.360	24.44	$2.14e-3$	10.27	−6.85
4#	522.182	145.982	22.57	3.61	−3.94	0.52
5#	518.066	156.619	20.95	2.44	−4.29	6.72
6#	449.424	108.787	35.30	−0.04	−1.63	5.22
7#	473.512	110.345	33.40	7.65	−0.62	−0.70
8#	495.898	111.733	31.82	8.13	1.23	−5.36
9#	516.942	113.001	30.45	−6.81	2.76	−9.58
10#	485.760	104.012	31.40	0.18	−0.72	−0.72
11#	512.631	109.363	30.23	4.54	−1.2	6.12
12#	558.926	118.538	28.44	9.63	0.94	7.54
13#	579.326	122.564	27.73	−1.91	−2.14	−1.19
14#	566.955	132.755	27.65	−0.73	−13.69	23.99
15#	609.105	161.844	25.66	−3.67	−9.97	22.02
16#	650.316	193.933	23.97	14.14	9.73	4.68
17#	690.684	229.043	22.52	−7.83	1.30	−16.58

Table 9: The wire rope size parameters used in the GGQ25-62 Polycal WRI [24].

Arc strand	Parameters	Value
Center strand	The diameter of the rope	1.64
	The diameter of core wire	0.36
	The diameter of lay wire	0.32
	The pitch length of the first layer	9.84
	The pitch length of the second layer	8.52
Lay strand	The diameter of the rope	1.52
	The diameter of lay wire	0.32
	The diameter of lay wire	0.30
	The pitch length of the first layer	9.12
	The pitch length of the second layer	7.93

Table 10: The structural parameters and stiffness-damping of the GGQ25-62 WRI.

	n_r	p_{in}/p_{out}	P/D	R/D	K_1 (N/mm)	K_2 (N/mm)	C (%)
Value	1.1	1.15	6.5	5.8125	199.98	58.57	35.86

5. Conclusion

This paper firstly presented the results of the mechanical properties of the wire rope with different diameter ratios and lay pitches of the single strand. By using the corrected simplified finite element method of the Polycal WRI, the influence of the diameter ratio and lay pitch of the single strand and the lay pitch and bending radius of the wire rope on the stiffness and damping characteristics of the Polycal WRI were studied. Several key conclusions are summarized as follows:

(1) The stiffness-damping characteristics were best; when the diameter ratio of wire strand was 1.1, the inside layer wire pitch length was 6 times the diameter of the wire strand, the outside layer wire pitch length was 11 times the diameter of the wire strand, the pitch length of the wire rope was 7.5 times its diameter, and the bending radius was equal to 46.5 mm.

(2) The effective prediction models of stiffness and damping about the structural parameters of the wire rope were established, which combined the properties of a steel wire material and the overall structure of the WRI. More than half of the errors of the prestiffness and softened stiffness fitting formulas of the Polycal WRI were within 5%. And more than half of the errors of the energy dissipation coefficient of the WRI were within 10%. The fitted value was compared with the experimental data, the errors were within 20%, and the prediction model was verified.

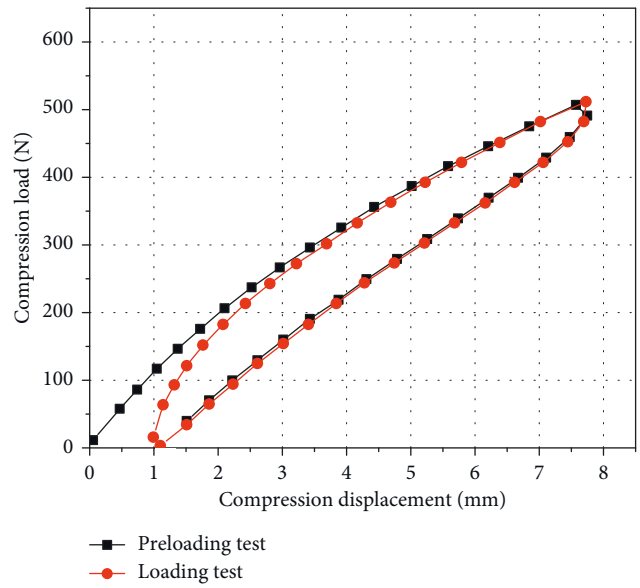

Figure 13: Experimental compression load-displacement results [24].

Table 11: Comparison between the fitted value and experimental data.

Result	K_1 (N/mm)	K_2 (N/mm)	C (%)
Fitted value	239.11	62.99	41.25
Experimental	199.98	58.57	35.86
Error	19.57%	7.55%	15.04%

Data Availability

The data used to support the findings of this study are available from the corresponding author upon request.

Conflicts of Interest

The authors declare that they have no conflicts of interest.

Acknowledgments

Financial supports from the National Natural Science Foundations of China (no. 11772147) and Natural Science Fund for Colleges and Universities in Jiangsu Province (16KJB130003) are gratefully acknowledged.

References

[1] J. Xi, Z. Feng, G. Wang, and F. Wang, "Vibration and noise source identification methods for a diesel engine," *Journal of Mechanical Science and Technology*, vol. 29, no. 1, pp. 181–189, 2015.

[2] H. Wang, J. Gong, and G. Chen, "Characteristics analysis of aero-engine whole vibration response with rolling bearing radial clearance," *Journal of Mechanical Science and Technology*, vol. 31, no. 5, pp. 2129–2141, 2017.

[3] M. Leblouba and S. Barakat, "Performance of wire rope isolators in the seismic protection of equipment," *MATEC Web of Conferences*, vol. 120, article 01009, 2017.

[4] S. Alessandri, R. Giannini, F. Paolacci, and M. Malena, "Seismic retrofitting of an HV circuit breaker using base isolation with wire ropes. Part 1: preliminary tests and analyses," *Engineering Structures*, vol. 98, pp. 251–262, 2015.

[5] S. Alessandri, R. Giannini, F. Paolacci, M. Amoretti, and A Freddo, "Seismic retrofitting of an HV circuit breaker using base isolation with wire ropes. Part 2: shaking-table test validation," *Engineering Structures*, vol. 98, pp. 263–274, 2015.

[6] N. Vaiana, M. Spizzuoco, and G. Serino, "Wire rope isolators for seismically base-isolated lightweight structures: experimental characterization and mathematical modeling," *Engineering Structures*, vol. 140, pp. 498–514, 2017.

[7] S. Rashidi and S. Ziaei-Rad, "Experimental and numerical vibration analysis of wire rope isolators under quasi-static and dynamic loadings," *Engineering Structures*, vol. 148, pp. 328–339, 2017.

[8] P. S. Balaji, L. Moussa, N. Khandoker, T. Y. Shyh, M. E. Rahman, and L. H. Ho, "Experimental study on vertical static stiffnesses of polycal wire rope isolators," *IOP Conference Series: Materials Science and Engineering Conference Series*, vol. 217, article 012032, 2017.

[9] R. R. Gerges, "Model for the force–displacement relationship of wire rope springs," *Journal of Aerospace Engineering*, vol. 21, no. 1, pp. 1–9, 2008.

[10] P. S. Balaji, L. Moussa, M. E. Rahman, and L. T. Vuia, "Experimental investigation on the hysteresis behavior of the wire rope isolators," *Journal of Mechanical Science and Technology*, vol. 29, no. 4, pp. 1527–1536, 2015.

[11] O. B. Simakov, I. K. Mikhalkin, and Y. K. Ponomarev, "Experimental research of ultra small vibration dampers for protection against vibration of memory units in automatic onboard systems on vehicles," *Procedia Engineering*, vol. 176, pp. 429–437, 2017.

[12] Y. Chen, F. Meng, and X. Gong, "Full contact analysis of wire rope strand subjected to varying loads based on semi-analytical method," *International Journal of Solids & Structures*, vol. 117, pp. 51–66, 2017.

[13] L. M. Tinker and M. A. Cutchins, "Damping phenomena in a wire rope vibration isolation system," *Journal of Sound and Vibration*, vol. 157, no. 1, pp. 7–18, 1992.

[14] G. F. Demetriades, M. C. Constantinou, A. M. Reinhorn, and M. Andrei, "Study of wire rope systems for seismic protection of equipment in buildings," *Engineering Structures*, vol. 15, no. 5, pp. 321–334, 1993.

[15] H.-X. Wang, X.-S. Gong, F. Pan, and X.-J. Dang, "Experimental investigations on the dynamic behaviour of O-type wire-cable vibration isolators," *Shock and Vibration*, vol. 2015, Article ID 869325, 12 pages, 2015.

[16] W.-G. Jiang, M. K. Warby, and J. L. Henshall, "Statically indeterminate contacts in axially loaded wire strand," *European Journal of Mechanics—A/Solids*, vol. 27, no. 1, pp. 69–78, 2008.

[17] H. Wang, C. Fu, W. Cui, X. Zhao, and S. Qie, "Numerical simulation and experimental study on stress deformation of braided wire rope," *Journal of Strain Analysis for Engineering Design*, vol. 52, no. 2, pp. 69–76, 2016.

[18] L. Xiang, H. Y. Wang, Y. Chen, Y. J. Guan, and L. H. Dai, "Elastic-plastic modelling of metallic strands and wire ropes under axial tension and torsion loads," *International Journal of Solids & Structures*, vol. 129, pp. 103–118, 2017.

[19] C. Yu, Y. Shuai, B. Dong, and Y. Bao, "The analysis of 91-wire strand tensile behavior using beam finite element model," *IOP Conference Series: Materials Science and Engineering*, vol. 381, article 012115, 2018.

[20] B. Song, H. Wang, W. Cui, H. Liu, and T. Yang, "Distributions of stress and deformation in a braided wire rope subjected to torsional loading," *Journal of Strain Analysis for Engineering Design*, vol. 54, no. 1, pp. 3–12, 2018.

[21] X. Cao and W. Wu, "The establishment of a mechanics model of multi-strand wire rope subjected to bending load with finite element simulation and experimental verification," *International Journal of Mechanical Sciences*, vol. 142-143, pp. 289–303, 2018.

[22] W. Du, B. Ma, D. Cao, and X. Zheng, "Finite element analysis on the stress state of rope hoisting equipment based on the ABAQUS," in *Proceeding of the 2017 8th International Conference on Mechanical and Intelligent Manufacturing Technologies (ICMIMT)*, Cape Town, South Africa, February 2017.

[23] H. Yong, Z. Hu, H. Ma, P. Yan, and L. Yuan, "Finite element simulation of axial elastic characteristics of wire rope with one round strand layer," in *Proceeding of the IEEE International Conference on Computer Supported Cooperative Work in Design*, Nanchang, China, May 2016.

[24] B. Cen, X. Lu, and X. Zhu, "Research of numerical simulation method on vertical stiffness of polycal wire rope isolator," *Journal of Mechanical Science and Technology*, vol. 32, no. 6, pp. 2541–2549, 2018.

[25] W. G. Jiang, J. L. Henshall, and J. M. Walton, "A concise finite element model for three-layered straight wire rope strand," *International Journal of Mechanical Sciences*, vol. 42, no. 1, pp. 63–86, 2000.

[26] C. Erdonmez and C. E. Imrak, "A finite element model for independent wire rope core with double helical geometry subjected to axial loads," *Sadhana*, vol. 36, no. 6, pp. 995–1008, 2011.